Supplemental materials to the manuscript "Disentangling microstructural elements of shear thickening suspensions via computer simulations of a minimal model"

I. FLOW CURVE

When constructing the flow curve, a single initial configuration was used for the system size of 20,000 particles. In contrast, for the system size of 2,000 particles a minimum of 5 statistically independent initial configurations was used for most rates. For both system sizes, data is taken by shearing the system until the shear stress reaches steady state. At that point, the system is sheared for an additional strain of $\Delta\gamma = 10$ and sampled in $\Delta\gamma = 0.001$ increments, resulting in 10,000 system configurations.

Figure 1 shows the flow curve for the two systems sizes. We find that for both sizes, quasi-Newtonian flow (QN) is observed at the lowest rates followed by thickening. Both the onset of thickening and of thinning seems to occur at slightly lower shear rates.

II. SHEAR STRESS FLUCTUATIONS

Figure 2 shows that the smaller system size of 2,000 particles exhibits larger variations in the stress than the 20,000 particle system. Interestingly, the smaller system size appears to alternate between low and high stress states, e.g. approximately between $0.5 \lesssim \Delta\gamma \lesssim 0.75$ in the figure. However, when the system size is increased this "switching"

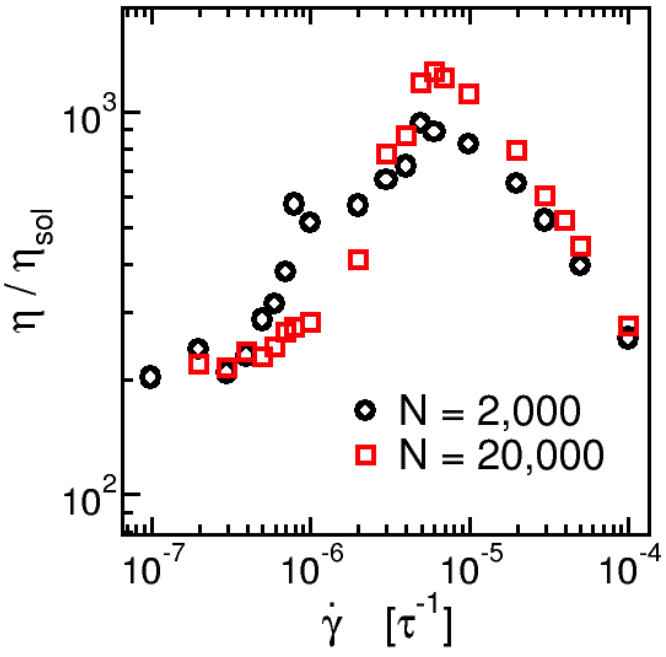

FIG. 1: System size comparison of the flow curve. Both system sizes exhibit a QN regime at the lowest observed rates followed by thickening and the onset of thinning at the same approximate rate ($\dot{\gamma}_P = 6 \times 10^{-6}\ \tau^{-1}$).

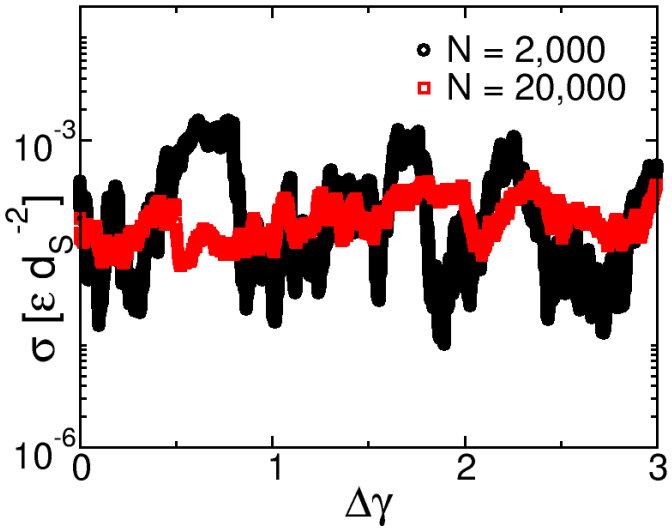

FIG. 2: Shear stress fluctuations at a shear rate of $\dot{\gamma} = 3 \times 10^{-6}\ \ \tau^{-1}$ for a system size of 2,000 and 20,000 disks. Strain values $\Delta\gamma$ are taken after the system has reached steady steady state. A qualitative change is seen with changing the system size.

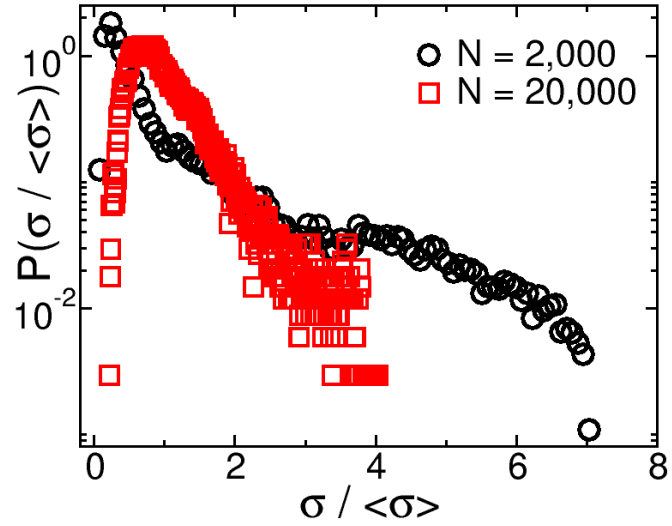

FIG. 3: Probability density distributions of the shear stress data shown in Figure 2

behavior disappears.This is also illustrated in Figure 3 which shows the probability density distribution for the data in Figure 2. When stresses are rescaled by their mean value, the data for the smaller system size exhibit a broad second peak at high stresses, whereas the data for the large system size feature an exponential tail and only one peak.

III. CLUSTER SIZE DISTRIBUTION

We identifies clusters (3-SFN) made of particles that have at least 3 contacts, each with a force satisfying $f > f_{peak}$ (3-SFN) where f_{peak} is the peak of the contact force distribution (CSD) for the shear rate being analyzed. To build the cluster size distribution n_s we count the number of such clusters that are made of s particles in each configuration and divide the result by the number of particles in the system. The data are collected and averaged over 10,000

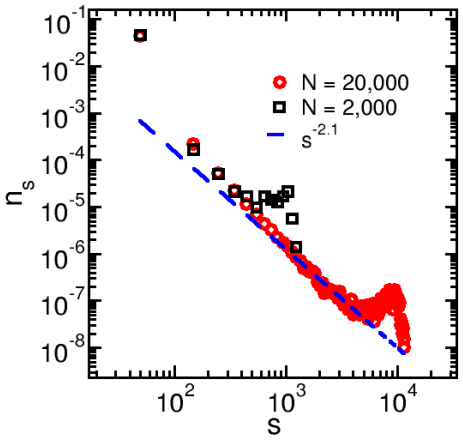

FIG. 4: Cluster size distribution of 3-SFN for two system sizes ($N = 2,000$ and $N = 20,000$ particles.) The y-axis represents the expected number of clusters at a given moment in time divided by the total number of particles while the x-axis gives the number of particles in the cluster. Data is for a shear rate in the thickening regime, $\dot{\gamma}' = 1.7 \times 10^{-1}$. The dashed line is a guid to the eye, showing a power law with an exponent ≈ 2.1, compatible with random percolation in $2d$.

configurations.

Figure 4 shows the 3-SFN cluster size distribution using two different system sizes for a rate in the thickening regime.

IV. 3-SFN AND PEBBLE GAME CLUSTERS

Figure 5 shows the average fraction of particles in percolating 3-SFN that are also in a rigid cluster according to the pebble game algorithm, for a few shear rates in the different rheological regimes. The two types of clusters have a large overlap during the quasi-Newtonian and thinning regimes. During thickening, percolating 3-SFN may have a significant fraction of particles that do not belong to pebble game clusters, but this fraction decreases with increasing shear rate.

Figure 6 shows that 3-SFN clusters of all sizes almost completely overlap with pebble game clusters during the QN and thinning regimes. In contrast, for the thickening flow, only the largest 3-SFN (those containing around 60% of the particles or more) have large overlap with the pebble game clusters.

Figure 7 compares the Pearson correlation coefficient between cluster percolation and the shear stress for 3-SFN and pebble game clusters. While the percolation of pebble game clusters correlate well with the shear stress with $r \approx 0.5 - 0.6$ at given rates, the correlation with 3-SFN is consistently higher throughout the thickening regime.

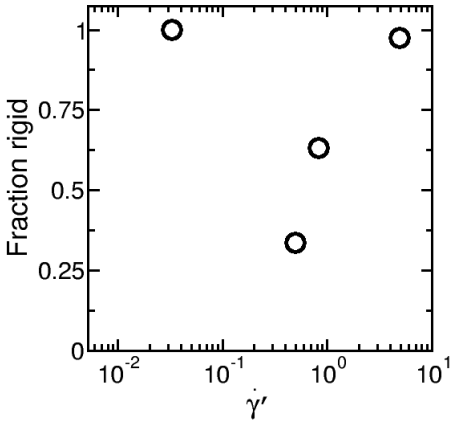

FIG. 5: The average fraction of particles in percolating 3-SFN that are rigid at various rates.

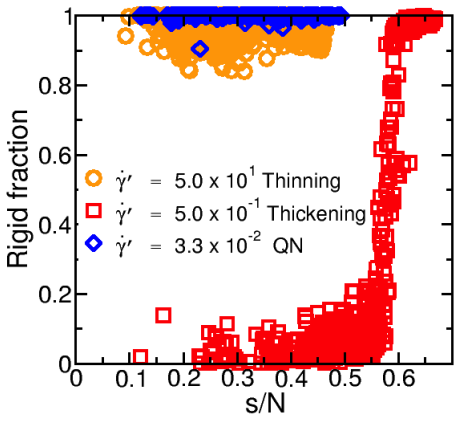

FIG. 6: The fraction of particles in individual percolating clusters that are rigid versus the size of that cluster s (expressed as a fraction of the total number of particles N) for various rates.

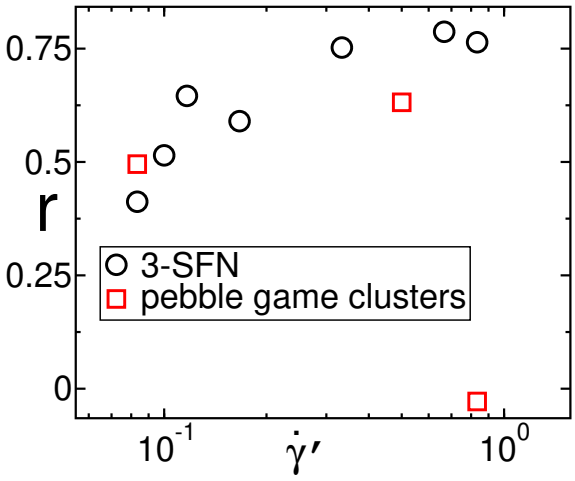

FIG. 7: The Pearson correlation coefficient between percolation status and the instantaneous shear stress. The 3-SFN networks appear correlate better with the shear stress, particularly deep into the thickening.